Quaternary Geochronology 4 (2009) 93–107

Contents lists available at ScienceDirect

Quaternary Geochronology

journal homepage: www.elsevier.com/locate/quageo

Research Paper

Regional beryllium-10 production rate calibration for late-glacial northeastern North America

Greg Balco [a,*], Jason Briner [b], Robert C. Finkel [c], John A. Rayburn [d], John C. Ridge [e], Joerg M. Schaefer [f]

[a] Berkeley Geochronology Center, 2455 Ridge Road, Berkeley, CA 94709, USA
[b] Geology Department, University at Buffalo, Buffalo, NY, USA
[c] University of California, Berkeley, CA, USA
[d] Geology Department, State University of New York at New Paltz, New Paltz, NY, USA
[e] Department of Geology, Tufts University, Medford, MA, USA
[f] Lamont-Doherty Earth Observatory, Palisades, NY, USA

ARTICLE INFO

Article history:
Received 17 March 2008
Received in revised form 9 September 2008
Accepted 24 September 2008
Available online 14 October 2008

Keywords:
Cosmogenic-nuclide geochronology
Beryllium-10
Aluminum-26
Massachusetts
New Hampshire
New York
Baffin Island
Last Glacial Maximum
Varve chronology
Deglaciation
Production rate calibration

ABSTRACT

The major uncertainty in relating cosmogenic-nuclide exposure ages to ages measured by other dating methods comes from extrapolating nuclide production rates measured at globally scattered calibration sites to the sites of unknown age that are to be dated. This uncertainty can be reduced by locating production rate calibration sites that are similar in location and age to the sites to be dated. We use this strategy to reconcile exposure age and radiocarbon deglaciation chronologies for northeastern North America by compiling ^{10}Be production rate calibration measurements from independently dated late-glacial and early Holocene ice-marginal landforms in this region. ^{10}Be production rates measured at these sites are 6–12% lower than predicted by the commonly accepted global ^{10}Be calibration data set used with any published production rate scaling scheme. In addition, the regional calibration data set shows significantly less internal scatter than the global calibration data set. Thus, this calibration data set can be used to improve both the precision and accuracy of exposure dating of regional late-glacial events. For example, if the global calibration data set is used to calculate exposure ages, the exposure-age deglaciation chronology for central New England is inconsistent with the deglaciation chronology inferred from radiocarbon dating and varve stratigraphy. We show that using the regional data set instead makes the exposure age and radiocarbon chronologies consistent. This increases confidence in correlating exposure ages of ice-marginal landforms in northeastern North America with glacial and climate events dated by other means.

Introduction

1.1. Cosmogenic-nuclide production rate measurements

Cosmogenic-nuclide exposure dating involves measuring the concentration of one of these nuclides in a rock surface to be dated, and then applying an independently measured nuclide production rate to transform the concentration measurement to an age. Thus, accurate exposure dating relies entirely on an accurate estimate of the production rate. Production rates vary with time and location, so estimating the average production rate during the period of exposure at a site of unknown age involves: (i) measuring the production rate at independently dated calibration sites, (ii) using a scaling scheme that describes the production rate variation with time and location to scale these measured local, time-integrated production rates to a common reference time and location (usually taken to be the present time at sea level and high latitude), (iii) averaging or otherwise summarizing the resulting estimates of the reference production rate, and (iv) using the same scaling scheme to scale this average reference production rate to the unknown-age site. If the scaling scheme correctly describes production rate variations and the calibration measurements are free of systematic errors, the estimates of the reference production rate obtained in (ii) above from widely scattered sites should agree within measurement error. Furthermore, as the production rate calibration sites have been independently dated (for the most part by calibrated radiocarbon dates) this procedure should ensure that exposure ages can always be accurately correlated with ages measured by other dating methods. However, reference production rates derived from the existing global calibration data set and any published scaling method display several times more scatter than can be explained by measurement error (see Balco et al. (2008), for details. Throughout this paper, by 'global calibration data set' we mean the data set described in this reference). In addition, the

* Corresponding author. Tel.: +1 510 644 9200.
E-mail address: balcs@bgc.org (G. Balco).

1871-1014/$ – see front matter © 2008 Elsevier Ltd. All rights reserved.
doi:10.1016/j.quageo.2008.09.001

differences among reference production rates computed from individual calibration sites are larger than the internal scatter of data from any particular site. This observation most likely requires both inaccuracies in the scaling schemes and systematic errors in the calibration data set. Both of these possibilities imply that the accuracy of exposure ages computed with any scaling scheme and the global calibration data set will vary significantly with age and location. Such exposure ages will be inaccurate for at least some locations and exposure times. The global calibration data set is dominated by calibration sites at mountain elevations and latitudes between 30 and 45 °N, so is expected to yield accurate exposure ages at unknown sites with these characteristics. However, estimating nuclide production rates at locations and exposure ages that are significantly different in latitude, elevation, or age requires using scaling schemes to extrapolate away from, rather than interpolate between, calibration measurements. This results in large differences between production rates predicted by different scaling methods, and very likely in large and difficult to estimate errors in any one of these production rate estimates. For the commonly used cosmogenic nuclide ^{10}Be, the scatter of reference production rates inferred from the existing global calibration data set suggests that the uncertainty in estimating ^{10}Be production rates at an arbitrary time and location exceeds 10% (Balco et al., 2008). Thus, ^{10}Be exposure ages calculated on the basis of this calibration data set cannot be confidently related to ages determined using other dating methods at better than the 10% level, and for times and locations that are not spanned by the calibration data set, scaling factor extrapolation may result in larger errors.

One way to reduce the importance of scaling uncertainties on cosmogenic-nuclide exposure ages, and thus increase the accuracy of exposure dating, is to locate production rate calibration sites that are similar in age and location to the sites of unknown age that one wishes to date. Then, scaling corrections between the calibration sites and the unknown-age sites are small, and scaling factor inaccuracies are minimized. Here we follow this approach to improve the accuracy of cosmogenic-nuclide exposure dating for late-glacial events in northeastern North America.

1.2. Deglaciation in northeastern North America

Accurate dating of late-glacial events in northeastern North America is important for several reasons: for example, changes in the marginal position of the Laurentide Ice Sheet (LIS) in this region controlled the routing of meltwater derived from a large portion of the LIS to the Atlantic Ocean, so understanding the timing of ice-marginal events that relate to meltwater routing is important in evaluating hypotheses about meltwater forcing of North Atlantic climate change (Broecker, 2006; Lowell et al., 2005; Rayburn et al., 2005). In addition, the existing deglaciation chronology for the eastern margin of the LIS suggests that the ice margin position also responded to North Atlantic climate changes (e.g. Balco et al., 2002; Lowell et al., 1999), suggesting the possibility of complicated feedback relationships between ice sheet and climate changes. Determining the sequence of these events, and using this information to evaluate hypotheses about feedback relationships, requires the use of many different dating methods, and these must all be linked to a common time scale. Several previous studies (Balco and Schaefer, 2006; Briner et al., 2007; Rayburn et al., 2007a) have noted that cosmogenic-nuclide exposure ages for late-glacial landforms in northeastern North America that were calculated using a global production rate calibration data set are inconsistent with radiocarbon dates. In this work, we seek to resolve this inconsistency and make progress toward the overall goal of accurate correlation of glacial and climate events.

The important point about northeastern North America from the perspective of cosmogenic-nuclide dating is that this region spans a relatively small elevation range, and is located at a latitude high enough that production rates are relatively insensitive to magnetic field variations. Thus, scaling corrections among late-glacial landforms in the region are small relative to the scaling corrections required to tie together the entire global calibration data set. In this situation, scaling uncertainties can be significantly reduced by using a local rather than global calibration data set. In the remainder of this paper, we compile a ^{10}Be production rate calibration data set for northeastern North America, show that reference production rates derived from this regional calibration data set differ significantly from reference production rates derived from the global calibration data set, and show that the new data set successfully reconciles exposure-age and radiocarbon deglaciation chronologies in an example from central New England.

1.3. Note on age units and usage

This paper describes: (i) radiocarbon dates, (ii) ages referenced to a floating varve chronology that has been calibrated to the calendar year time scale by radiocarbon dating, and (iii) cosmogenic-nuclide exposure ages. All the radiocarbon dates we refer to in this paper have been published elsewhere, and are not the subject of this work. We have calibrated all of these radiocarbon dates to calendar years using the INTCAL04 calibration (Reimer et al., 2004). For simplicity, we state these radiocarbon ages only as calibrated ages with units of calibrated years before 1950 (cal yr BP). Readers are referred to the source papers for the measured ^{14}C concentrations. We also estimate the offset between the floating New England varve chronology (described below) and true calendar years using radiocarbon dates calibrated with INTCAL04. Thus, deglaciation ages derived from the varve chronology are consistent with calibrated radiocarbon ages, and we also state them in units of cal yr BP. We state exposure ages in units of years. The fact that radiocarbon ages are referenced to 1950, while exposure ages and nuclide production rates are referenced to the time of measurement, introduces a small inconsistency into the production rate calibration process. Following common practice, we have not dealt with this explicitly. All uncertainties in this paper are stated at one standard error.

2. Deglaciation chronologies in northeastern North America

The chronology of Laurentide Ice Sheet retreat in northeastern North America is based on: (i) terrestrial and marine radiocarbon dates from ice-proximal and postglacial deposits, (ii) varve chronology, and (iii) cosmogenic-nuclide exposure dating.

Terrestrial radiocarbon dates pertinent to deglaciation are, with few exceptions, minimum ages derived from pond bottoms, bog bottoms, or other organic sediments directly overlying glacial deposits. The majority of such radiocarbon dates are summarized in Borns et al. (2004) and Stone and Borns (1986) for New England, and in Dyke et al. (2003) for Canada. The vast majority of postglacial radiocarbon ages in northeastern North America are younger than 15,000 cal yr BP, even though the LIS began to retreat from its terminal position thousands of years earlier. This phenomenon presumably reflects the relatively low abundance of organic matter, and the long lag time between deglaciation and significant organic matter accumulation, in the cold environment that prevailed in ice-marginal regions prior to major North Atlantic climate warming ca. 15,000 cal yr BP. Its effect is that ice-marginal deposits in southern New England, that record events between approximately 25,000 and 15,000 years ago, cannot in general be radiocarbon dated.

Large regions of coastal New England and Atlantic Canada were submerged during deglaciation due to glacial isostatic depression and consequent marine flooding during deglaciation. Thus, ice-proximal glaciomarine sediment containing radiocarbon-dateable

marine fossils is common, and much of the regional deglaciation chronology is based on marine radiocarbon ages. In order to make marine and terrestrial radiocarbon chronologies consistent one must correct for the so-called marine reservoir effect, which reflects the fact that the marine carbon pool is depleted in ^{14}C relative to the atmospheric carbon pool. The marine reservoir correction in some parts of northeastern North America during deglaciation was larger than present, changed rapidly over time, and has not yet been accurately reconstructed. This is the presumed cause of observed discrepancies of several hundred years between regional marine and terrestrial radiocarbon chronologies for deglaciation. Ridge et al. (2001) and Borns et al. (2004) discuss the marine reservoir effect in New England in detail.

The deglaciation chronology for much of the northeast U.S. can also be inferred from the New England varve chronology (NEVC). There are north-draining valleys throughout New England, many south-draining valleys were dammed by glacial sediment during deglaciation, and the entire landscape was glacioisostatically tilted toward the center of the ice sheet to the north. Thus, there were proglacial lakes throughout New England during and well after deglaciation. The largest and longest-lasting of these was glacial Lake Hitchcock, which was initially created by ice retreat from a sediment dam in central Connecticut, survived several subsequent spillway changes, and continuously occupied at least some part of the Connecticut River Valley for approximately 6000 years. The lake-bottom sediments that record the presence of Lake Hitchcock and many other lakes contain annual laminations, that is, varves, and varved sediment sections throughout New England have been matched to assemble several long sequences that serve as a tool for high-resolution time correlation of late-glacial events. These varve sequences serve as a precise deglaciation chronology as well: not only does the existence of a particular varve at a certain site show that the site must have been ice-free in the year represented by that varve, but many varves can be traced to their northern termination in ice-proximal sediments, thus showing the position of the ice margin in a particular varve year. The bulk of the NEVC is based on sections in glacial Lake Hitchcock that were originally described and correlated by Antevs (1922, 1928). Antevs developed two floating varve sequences from the lower (southern) and upper (northern) Connecticut River Valley, reflecting arbitrarily numbered New England varve years 2701–7750 (the numbering scheme runs forward, so that younger varves have higher numbers). The designations 'lower' and 'upper' for the two parts of the NEVC defined by Antevs refer to both stratigraphic position and location in the Connecticut valley: the lower sequence is both downriver from and stratigraphically below the upper sequence. Antevs also matched these sequences to other, shorter, varve sequences in the Hudson, Merrimack, and Winooski Valleys of New York, New Hampshire, and Vermont, respectively. Later work by Ridge and co-workers (Ridge and Larsen, 1990; Ridge et al., 2001; Ridge, 2003, 2004; Rittenour et al., 2000; Ridge and Toll, 1999) extended the NEVC to cover NE varve years 2701–8679, matched it to additional varve sequences in Maine, and correlated it with glaciolacustrine sections in the Champlain Valley and the western Mohawk Valley of New York via paleomagnetic declination measurements. Finally, recent work by Ridge and co-workers has matched the upper and lower Connecticut Valley sequences (Ridge, 2008), resulting in a single 5600-year sequence. This matching requires a discussion of the numbering system of the two parts of the NEVC originally defined by Antevs. Antevs originally estimated the duration of the gap between the uppermost varve in the lower NEVC and the lowermost varve in the upper NEVC from the rate of ice recession before and after the gap. Ridge (2008) matched the two sections and found that Antevs had overestimated the duration of this gap by 332 years. In addition, Rittenour (1999) found 10 spurious varves, that were in fact flood deposits and not varves, near the top of Antevs' lower NE varve chronology. In this paper, we follow common practice and continue to refer to NE varve years using the original numbering system of Antevs. Thus, an NE varve age that belongs to the upper chronology must be reduced by 342 years for comparison to varve years that belong to the lower chronology. This issue is confusing and we have attempted to be as specific as possible throughout this paper.

The NEVC has been linked to the calibrated radiocarbon time scale by 41 radiocarbon dates on organic material found within individual varves or sets of varves (these are tabulated in Ridge (2003), Ridge (2004), and Ridge (2008)). Ridge (2008) rejected 14 of these dates on the basis either of relatively poor measurement precision, poor agreement between aliquots of the same sample, or sample material (such as large pieces of wood) of uncertain origin or that could have been recycled from older deposits, leaving 27 radiocarbon dates. Here we represent the varve year – calibrated radiocarbon year relationship by a value for the offset between the two: the offset is the calibrated radiocarbon year age of the varve with NE varve year zero. Taking calibrated radiocarbon years before present to be negative, subtracting the offset from the NE varve year of a particular varve yields the age of the varve in cal yr BP. In this work, we obtain the offset by choosing the value that results in the best fit (formally, that minimizes the error-weighted sum of squares) between the measured radiocarbon dates and the INTCAL04 radiocarbon calibration curve. This yields an offset of $20{,}770 \pm 100$ yr (here we define the offset as the age of the zero varve, so it applies to varve years in the lower NE varve chronology. NE varve years that belong to the upper varve chronology must be adjusted, as discussed above, before applying the offset). However, this uncertainty estimate assumes that the INTCAL04 calibration curve is correct in the time range of interest. For example, the alternative radiocarbon calibration curve between 12,500 and 13,000 cal yr BP of Muscheler et al. (2008) improves the fit between the radiocarbon dates from the NEVC and the radiocarbon calibration curve, and lowers the best-fit value of the offset to 20,700 yr. To account for this ambiguity, in this work we take the varve year – calibrated radiocarbon year offset to be $20{,}750 \pm 200$ yr; this fixes the NEVC to the time period between 18,050 and 12,410 cal yr BP. To summarize, events during deglaciation can be correlated across a large area of the eastern U.S. through the varve chronology, many ice-marginal deposits in New England can be stratigraphically linked to particular varves or sets of varves, and these varves can be linked to the calendar year time scale by the varve year – calibrated radiocarbon year offset determined from the radiocarbon data set.

Finally, the oldest terrestrial ice-marginal deposits in the region, the moraine systems in southern New England that were emplaced between approximately 25,000 and 18,000 years ago, have been dated by cosmogenic-nuclide exposure dating (Balco et al., 2002; Balco and Schaefer, 2006). Sets of exposure ages from most of these moraines are internally consistent and show little scatter, resulting in a nominal measurement uncertainty in the age of some individual moraines of less than 2%. However, in previous work (Balco and Schaefer, 2006), we showed that these exposure ages, which were calculated using the global production rate calibration data set described in Stone (2000) and Balco et al. (2008), were almost certainly incorrect, because they were significantly younger than permitted by the stratigraphic relationship between the moraines, the NEVC, and radiocarbon-dated postglacial sediments. We proposed that this inconsistency could be resolved by revising the ^{10}Be production rate used to calculate the exposure ages, but did not present any means of determining what the correct production rate was. In this paper we correct that omission.

To summarize, (i) the New England varve chronology and the terrestrial radiocarbon chronology have been intercalibrated and yield consistent ages where they overlap; (ii) the terrestrial and

marine radiocarbon chronologies may be inconsistent because of errors in the marine reservoir correction; and (iii) the exposure-age deglaciation chronology calculated using the global production rate calibration data set has been shown to be inconsistent with the terrestrial radiocarbon and varve chronologies. In this paper we resolve (iii).

3. The calibration sites

We measured ^{10}Be concentrations in boulders on ice-marginal landforms at the Littleton Moraine in New Hampshire ($n = 4$), at several other sites in the upper Connecticut River Valley of Massachusetts and New Hampshire ($n = 8$), at the Cobblestone Hill proglacial lake outlet channel near Altona, NY ($n = 7$), and at the Clyde River fjord head, Baffin Island, Nunavut, Canada ($n = 7$) (Table 1; Fig. 1).

3.1. Littleton Moraine near Littleton and Bethlehem, NH

The Littleton–Bethlehem moraine complex is a series of boulder-covered ridges that were emplaced by the retreating Laurentide Ice Sheet on the northern flank of the White Mountains. Thompson et al. (1996), Thompson et al. (1999), and Thompson et al. (2002) describe the moraine complex in detail. The moraine system can be traced west into the Connecticut River valley (Fig. 2), where it is correlated with a till that is both underlain and overlain by varved glaciolacustrine sediments (Ridge et al., 1996, 1999). The varve sections have been matched with the New England varve chronology, indicating that the till, and by extension the Littleton–Bethlehem moraine complex, was emplaced between NE varve years 7154 and 7305 (Ridge et al., 1999; Antevs, 1928; Lougee, 1935). In addition, unusually thick varves between NE varve years 7200 and 7214 appear to record drainage of proglacial lakes upon initial ice recession from the moraine complex (Ridge et al., 1999). Thus, boulders on the Littleton–Bethlehem moraines were exposed by ice recession between NE varve years 7200 and 7300. This range of varve years belongs to the upper NE varve chronology, so is equivalent to 6858–6958 in the lower varve chronology; with the value of the offset given above this corresponds to 13,790 ± 200–13,890 ± 200 cal yr BP. To facilitate error propagation we take this as 13,840 ± 250 cal yr BP.

We collected boulders from two sites in the Littleton–Bethlehem moraine complex (Fig. 2; Table 1) – the Sleeping Astronomer moraine (06-NE-010-LIT and 06-NE-011-LIT) and the Beech Hill

Table 1
Sample locations and cosmogenic-nuclide measurements. The samples from Clyde Inlet are also described in Briner et al. (2007); however, the ^{10}Be concentrations reported here differ slightly from those reported in that paper because we used a larger sample of blank measurements to calculate long-term average process blank corrections.

Sample name	Latitude (DD)	Longitude (DD)	Elevation (m)	Boulder size (L × W × H) (m)	Thickness (cm)	Shielding correction	Laboratory[a]	[^{10}Be] (10^3 atoms g^{-1})	[^{26}Al] (10^3 atoms g^{-1})	Independently determined exposure age (years)
Littleton moraine										
06-NE-010-LIT	44.2903	−71.7612	357	4 × 2.3 × 1.8	2	0.999	UW	81.8 ± 2.6	447 ± 29	13,840 ± 250
06-NE-011-LIT	44.2904	−71.7608	357	4.5 × 3.3 × 1.9	2	0.999	UW	80.6 ± 2.7	514 ± 36	13,840 ± 250
06-NE-012-LIT	44.3129	−71.5722	414	3.2 × 2.2 × 1.6	1	0.999	UW	88.3 ± 2.3	559 ± 25	13,840 ± 250
06-NE-013-LIT	44.3146	−71.5730	412	2.2 × 2 × 1.6	10	0.999	UW	86.1 ± 2.4	498 ± 20	13,840 ± 250
							LDEO	74.0 ± 2.8	–	13,840 ± 250
							Average	81.0 ± 1.8	498 ± 20	13,840 ± 250
Central CT River Valley										
06-NE-001-HOL	42.3039	−72.5319	304	1.5 × 2 × 0.8	1	1	UW	105.7 ± 4.8	–	16,750 ± 320
06-NE-002-LEV	42.5042	−72.5224	135	3.5 × 2.5 × 1.8	5	0.998	UW	84.0 ± 2.2	–	15,850 ± 300
							UW	75.3 ± 2.7	–	15,850 ± 300
							Average	80.4 ± 1.7	–	15,850 ± 300
06-NE-003-LEV	42.5059	−72.5212	160	2 × 2.5 × 1	3	0.999	UW	87.1 ± 2.2	–	15,850 ± 300
06-NE-004-LEV	42.5049	−72.5218	154	1 × 1.2 × 0.9	2	0.999	UW	91.1 ± 2.6	–	15,850 ± 300
06-NE-005-ASH	43.0146	−72.3251	180	3.6 × 2.4 × 1.6	6	0.999	UW	72.0 ± 2.2	–	15,100 ± 300
							UW	74.6 ± 2.0	–	15,100 ± 300
							Average	73.4 ± 1.5	–	15,100 ± 300
06-NE-006-ASH	43.0146	−72.3266	184	3 × 2.5 × 1.3	4	0.999	UW	69.2 ± 1.9	–	15,100 ± 300
							UW	76.2 ± 2.0	–	15,100 ± 300
							LDEO	71.7 ± 4.2	–	15,100 ± 300
							Average	72.3 ± 1.3	–	15,100 ± 300
06-NE-008-PER	43.2766	−72.3581	303	2 × 1.1 × 0.6	3	0.998	UW	33.3 ± 1.2	–	14,590 ± 230
06-NE-009-PER	43.2765	−72.3581	303	1.2 × 1 × 0.8	6	0.998	UW	79.9 ± 2.9	374 ± 51	14,590 ± 230
Cobblestone Hill										
CH-1	44.8460	−73.5790	237	3 × 1.5 × 1	2	1	UB	64.9 ± 10.6	–	13,180 ± 130
CH-2	44.8460	−73.5790	236	2.5 × 1.5 × 1	1	1	UB	60.7 ± 6.5	–	13180 ± 130
CH-3	44.8430	−73.5770	226	3 × 3 × 2	2	1	UB	58.7 ± 3.5	–	13,180 ± 130
CH-4	44.8430	−73.5770	226	4 × 3 × 1	2.5	1	UB	66.4 ± 4.1	–	13,180 ± 130
CH-5	44.8430	−73.5750	226	3 × 3 × 1.5	3	1	UB	65.9 ± 4.1	–	13,180 ± 130
CH-6	44.8430	−73.5750	226	4 × 2 × 1	2.5	1	UB	67.7 ± 4.3	–	13,180 ± 130
CH-7	44.8650	−73.6620	259	n/a[b]	1	1	UB	70.9 ± 12.1	–	13,180 ± 130
Clyde Inlet										
CI2-01-01	69.8353	−70.4970	65	1.5 × 1.5 × 2	5	1	CU	35.9 ± 3.9	–	8100 ± 250
CI2-01-02	69.8345	−70.4980	65	3 × 3 × 2	4	1	CU	38.3 ± 3.8	–	8100 ± 250
CR03-90	69.8302	−70.4962	72	2 × 2 × 1.3	2	1	CU	40.2 ± 3.4	–	8100 ± 250
CR03-91	69.8318	−70.4958	67	2.1 × 2.1 × 1.1	2	1	CU	37.0 ± 3.0	–	8100 ± 250
CR03-92	69.8318	−70.4958	67	3.2 × 3.2 × 1.5	2	1	CU	40.2 ± 2.6	–	8100 ± 250
CR03-93	69.8324	−70.4967	67	2.2 × 2.2 × 1.6	3	1	CU	41.1 ± 2.3	–	8100 ± 250
CR03-94	69.8328	−70.4975	65	3 × 3 × 1.3	2	1	CU	42.3 ± 2.9	–	8100 ± 250

[a] UW: University of Washington; LDEO: Lamont-Doherty Earth Observatory; CU: University of Colorado; UB: University at Buffalo.
[b] Not applicable: bedrock surface sample.

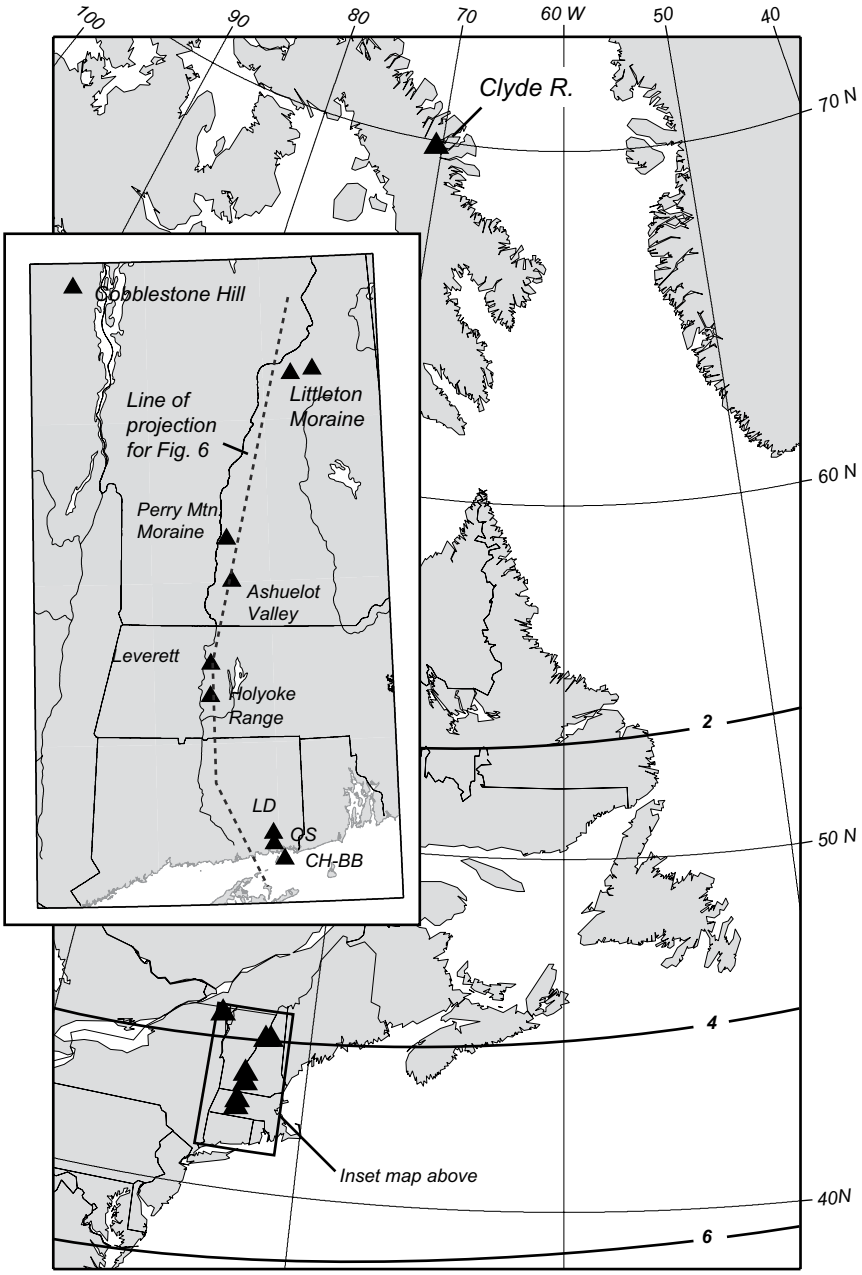

Fig. 1. Site locations. The dark lines show contours of geomagnetic cutoff rigidity (GV) averaged over the past 7000 yr (Lifton et al., 2008).

moraine field (06-NE-012-LIT and 06-NE-013-LIT). These sites are described in Thompson et al. (1996) and Thompson et al. (2002). The boulders at the Sleeping Astronomer moraine are weakly foliated quartz-plagioclase-biotite gneiss, and are roughly tabular in shape. They are embedded in a rocky diamict and commonly occur in interlocking groups. The surfaces of the boulders are rough at a horizontal scale of several centimeters and a vertical scale of ~1 cm. They are lichen-covered and show a thin (<1 mm) oxidation rind, but lack evidence of flaking or spalling and ring when struck by a hammer. The boulders at the Beech Hill site are tabular in shape and composed of coarse-grained pink granite. Boulders at this site are densely clustered, and, in fact, the overall deposit consists mainly of a clast-supported interlocking boulder accumulation. The boulders we sampled lay on top of and were interlocked with other boulders. The surfaces of the boulders display ~0.5–1 cm roughness at a horizontal scale of a few centimeters. At the Beech Hill site, xenoliths were weathered 0.5–1 cm below the overall rock surface on several boulders. We observed one upstanding quartz vein on a boulder surface which had 0.7–1.5 cm relief. The surfaces show no weathering rind or evidence of flaking or spalling, and ring when struck by a hammer. We conclude that the boulders on this moraine experienced 0.5–1.5 cm of surface erosion since emplacement. Many boulders at both sites were covered by lichen and up to 5 cm of moss, and we observed a few boulders on which small trees were rooted in the moss.

3.2. Perry Mountain moraine

The Perry Mountain moraine is a small, gently sloping end moraine, the extension of which can be traced into the basin of glacial Lake Hitchcock (Ridge, 2001), where it can be correlated with the NEVC. Interpolation between the locations of basal/ice-proximal varves indicates that the moraine was emplaced near NE varve year 6500 in the upper varve chronology (Fig. 2). Note that

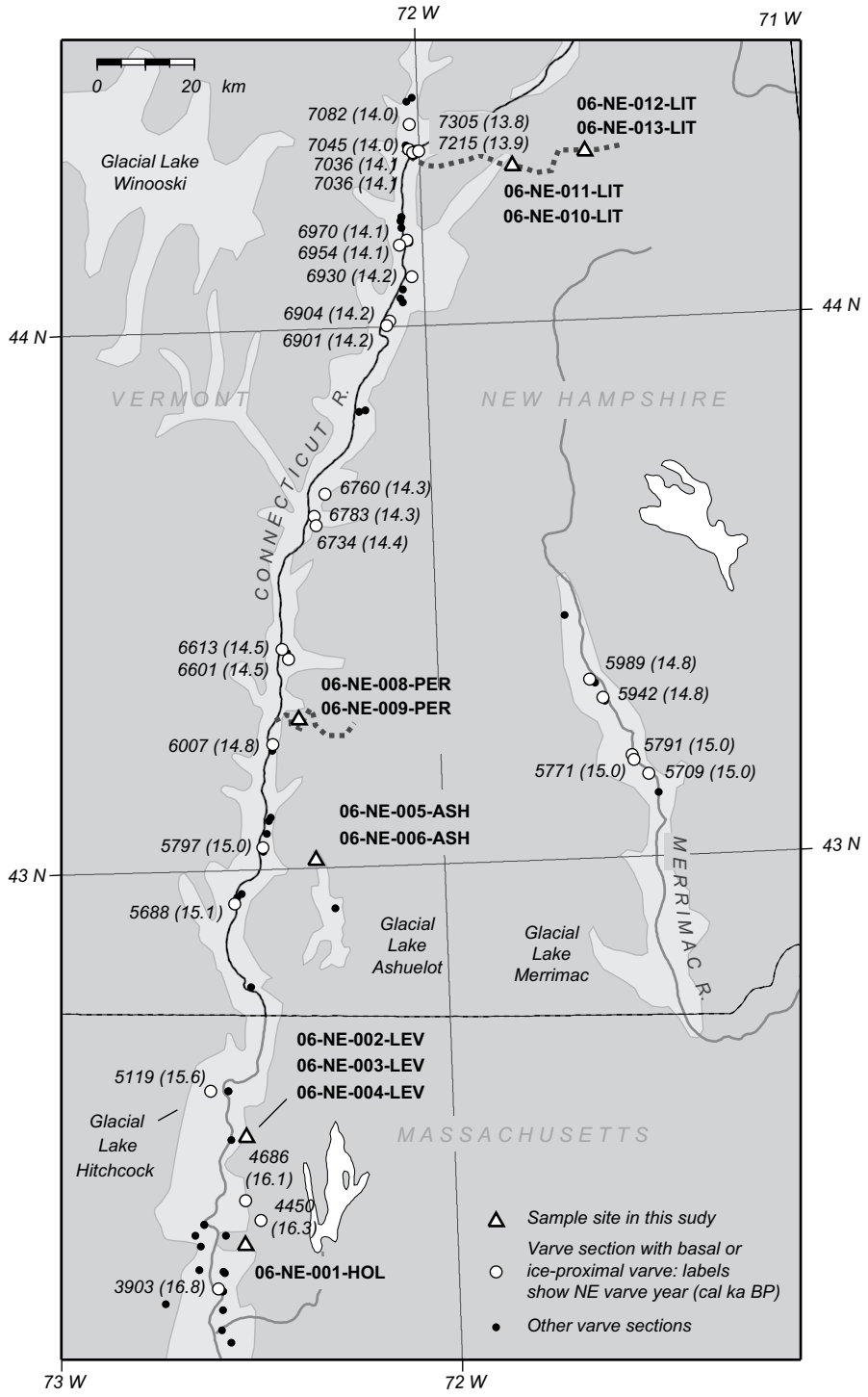

Fig. 2. Relationship between cosmogenic-nuclide sample sites in the Connecticut River Valley and the New England varve chronology. The labeled triangles show the location of cosmogenic-nuclide sample sites. The circles show the locations of varve sections from Antevs (1922, 1928) and Ridge et al. (1996). The white circles show sections where a basal or ice-proximal varve is exposed, thus indicating the location of the ice margin in a particular varve year, and the adjacent numbers show the New England varve year of that varve and the corresponding age of the varve in cal ka BP. Dark circles show other varve sections where no basal or ice-proximal varve is exposed. The heavy dotted lines show the approximate trace of the Littleton–Bethlehem moraine complex and the Perry Mountain moraine. The light shaded regions show the maximum extent of major glacial lakes.

deglaciation of this region was rapid – 90 m a^{-1} before emplacement of the Perry Mountain and related moraines, and 230 m a^{-1} shortly thereafter. Thus, even large geographic uncertainties in correlating upland ice-marginal deposits with varve sections only result in small uncertainties in the varve year deglaciation age of the upland deposits. This moraine lies ~10 km from the nearest varve sections, suggesting an uncertainty in its varve year age of ±50 years. With the value of the varve year–calendar year offset described above, the Perry Mountain moraine was exposed by ice retreat 14,590 ± 230 cal yr BP.

We sampled two boulders on this moraine. The moraine surface was flat to gently sloping and showed no evidence of degradation. 06-NE-009-PER is a fine-grained pink granite with a rough surface, but no perceptible weathering rind or evidence of flaking or

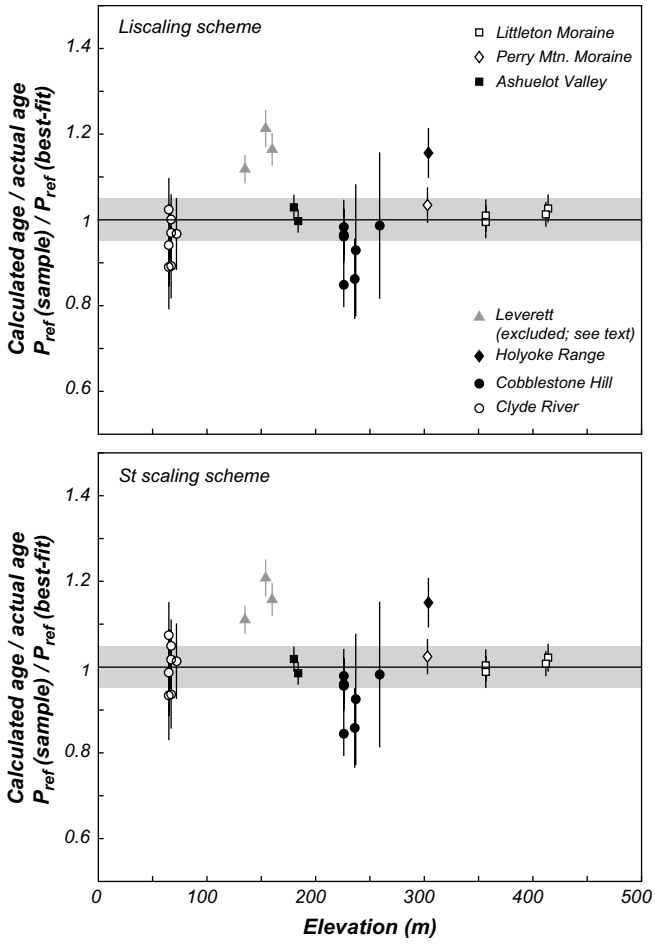

Fig. 3. Fit of representative scaling schemes to the regional calibration data set. The St scheme (the two-letter scaling scheme designations follow Balco et al. (2008)) is the non-time-dependent scaling of Stone (2000) following Lal (1991); the Li scaling scheme is that of Lifton et al. (2005) as implemented in Balco et al. (2008), which includes time-dependent magnetic field and solar effects on the production rate. Other time-dependent scaling schemes based on neutron-monitor data (those of Dunai (2001) and Desilets et al. (2006)) yield equivalent results to the Li scaling scheme for this data set. Each data point shows the ratio of the exposure age calculated from the ^{10}Be measurement at a calibration site, using the best-fitting reference production rate in Table 2, to the independently determined exposure age of the site. As all the calibration sites are young relative to the ^{10}Be half-life, this is equivalent to the ratio of the reference production rate inferred from a particular site and the reference production rate that best fits the entire data set. The error bars reflect 1σ uncertainties. The gray band reflects the 1σ uncertainty in the best-fit reference production rate from Table 2. There is no particular significance to the choice of elevation as the independent variable other than that it effectively spreads out the data for good readability, and facilitates comparison to similar plots in other work.

spalling. It rested on top of other boulders in a clast-supported, interlocking pile. 06-NE-008-PER is a tabular quartz-biotite schist boulder. The surface of the boulder appeared unweathered, and was not spalled or splintered. However, the nominal exposure age of this boulder calculated from our ^{10}Be measurement was only ~5500 years. Subsequent examination of field photos of this boulder showed that it did not appear to be interlocked with or even close to other boulders, and was embedded in silty soil. In northern New England, boulders in matrix-supported, fine-grained soils are pushed to the surface by frost heave, in a process so common as to be taken as emblematic of the Sisyphean labors faced by New Hampshire farmers (Frost, 1915). It appears that this boulder is no exception, and was pushed to the surface by frost heave thousands of years after deglaciation. We should have identified this condition in the field, should not have sampled this boulder, and disregard it for the remainder of this paper.

3.3. Ashuelot River Valley near Surry, NH

We collected samples 06-NE-005-ASH and 06-NE-006-ASH from a site where boulders lying on thin soil and bedrock outcrop are exposed in an ice-marginal drainage channel near the shore of glacial Lake Ashuelot. Nearby basal/ice-proximal varve locations were deglaciated between NE varve years 5600 and 5800. By similar reasoning as above, our best estimate of the deglaciation age in varve years is 5650 ± 170. This range of varve years belongs to the lower NE varve chronology. Thus, the site was exposed 15,100 ± 300 cal yr BP. These boulders are quartz–feldspar–biotite gneiss. They lie on flat ground, embedded in thin soil overlying bedrock ledges. Boulder surfaces are rough, and quartz pods stand in 0.5 cm relief. No weathering rind is present.

3.4. Spillway at Leverett, MA

This site is located in an ice-marginal drainage spillway feeding a prominent delta graded to glacial Lake Hitchcock (Mattox, 1951). The site is bracketed between basal/ice-proximal varves with ages of 4686 and 5119 NE varve years (Fig. 2). This range of varve years belongs to the lower NE varve chronology, so this site was deglaciated at 15,850 ± 300 cal yr BP. At this site, quartz–muscovite gneiss boulders, of matching lithology to the underlying bedrock, are scattered on top of bedrock ledges and thin soil. This suggests that the boulders were detached by subglacial plucking or ice-marginal drainage, but not transported an appreciable distance. We collected three boulders (06-NE-002-LEV, 06-NE-003-LEV, and 06-NE-004-LEV), all of which rested directly on bedrock. 06-NE-004-LEV was precariously balanced on a streamlined bedrock knob and could easily be rocked by hand. Boulder surfaces were lichen-covered and rough, and quartz veins stood up to 1 cm in relief. The boulders we sampled had an oxidation rind up to 5 mm thick, but showed no evidence of flaking or spalling.

3.5. Holyoke Range near Amherst, MA

The Holyoke Range is a basalt ridge that stands ~250 m above Mesozoic sediments in the Hartford Graben. The ridgetop surface is glacially streamlined, polished, and striated columnar basalt. The deglaciation age of the site is bracketed by basal/ice-proximal varves with ages of 3903 and 4450 NE varve years (Fig. 2). As the site is 200 m above the valley floor, it likely deglaciated somewhat before the adjacent glacial lake basin. Thus, we take the deglaciation age of this site to be 3800–4200 NE varve years in the lower NE varve chronology, or 16750 ± 320 cal yr BP. We sampled one erratic boulder (06-NE-001-HOL) of arkosic conglomerate that lay directly on the striated basalt ridgetop. The surface of the boulder was rough at the grain scale but hard and compact, with no evidence of flaking or spalling. Surface weathering was confined to a ~1–2 mm oxidation rind.

3.6. Cobblestone Hill spillway, NY

Cobblestone Hill is a flood bar immediately downstream of an ice-marginal channel through which glacial Lake Iroquois, a proglacial lake in the Lake Ontario basin, drained into glacial Lake Vermont, a proglacial lake in the Lake Champlain basin, following ice recession from the northern flank of the intervening Adirondack Mountains. The resulting flood was large – ca. 600 km^3 with an estimated flow velocity >8 m s^{-1} – and the flood channel is marked by a prominent gorge and a large (2.5 km long, 0.5 km wide and 15 m high) bar composed of meter-scale sandstone boulders that are imbricated in places. The site and the flood history are described in detail in Rayburn et al. (2005), Franzi et al. (2002), and Franzi et al. (2007). The flood must postdate radiocarbon-dated material

from Lake Iroquois sediments, the youngest of which is 13,438–13,020 cal yr BP. It must predate a resulting drop in the level of glacial Lake Vermont, that in turn must predate organic sediments from a pond isolated by this lake-level drop dated at 12,995–12,793 cal yr BP (Rayburn et al., 2007b). It must also predate the eventual drainage of Lake Vermont and establishment of marine conditions in the Champlain Sea that has been dated at 13,187–12,872 cal yr BP (Richard and Occhietti, 2005) and 13,124–12,853 cal yr B.P (Franzi et al., 2007). Finally, Rayburn et al. (2008) suggested that a series of sandy varves in Lake Vermont that record the Lake Iroquois breakout flood may match the (upper) New England varve chronology near NE varve year 7800; with the offset discussed above, this agrees with the radiocarbon age constraints and suggests an age near 13,300 cal yr BP. A maximum likelihood estimate based on the limiting calibrated radiocarbon ages noted above yields a 1σ age range of 13,316–13,051 cal yr BP for the flood. We take this to be the actual exposure age of Cobblestone Hill. For ease of error propagation we approximate this age as $13{,}180 \pm 130$ cal yr BP.

We sampled six boulders (samples CH-1 to CH-6) from the Cobblestone Hill boulder bar itself, and one glacially scoured bedrock surface near the presumed source area of the Cobblestone Hill boulders (CH-7). All consist of Potsdam Sandstone, a silica-cemented quartz sandstone with minor accessory minerals. The boulder deposit at Cobblestone Hill is composed of interlocking boulders up to 1–2 m high and 1–4 m in diameter; we selected relatively large boulders that were otherwise representative of the overall population. Lichen and moss are common on boulder surfaces. Boulder surfaces were hard, well cemented, and showed no visible weathering rind. This site is located within a pine barren. Vegetation is sparse, soils are thin to absent, and the dominant tree species is jack pine (*Pinus banksiana*). As this species requires fire to reproduce, it is certain that there have been many forest fires at this site since deglaciation. Thus, we looked carefully for evidence of thermal spalling of the boulders we sampled, but found no indication that they were affected by this process. The bedrock surface showed glacial polish and chatter marks, and was presumably exposed by deglaciation immediately prior to the outburst flood and emplacement of Cobblestone Hill. Bedrock surfaces nearby are covered by 2–5 cm of moss and soil. The sample site is near a road where it may have been disturbed during road grading, so it is very likely that it was covered by similar thin surface debris in the past.

3.7. Clyde River delta, Baffin Island

This site is a prominent ice-contact glaciomarine delta 62 m above sea level near the head of Clyde Inlet, eastern Baffin Island. Briner et al. (2007) describe the site, the samples, and their geologic context in detail. The delta is stratigraphically bracketed between marine sediments containing bivalves that have been radiocarbon dated. Given the marine reservoir correction of 540 years suggested by Briner et al. (2007) and the INTCAL04 radiocarbon calibration (Reimer et al., 2004), the delta must: (i) be younger than the youngest of several bivalves, dated at 8410–8370 cal yr BP, in a higher and stratigraphically older delta, and (ii) be older than several bivalves, dated at 7960–7870, 7960–7800, and 7790–7680 cal yr BP, in stratigraphically younger marine sediments. We conclude that the delta was abandoned 8100 ± 250 cal yr BP. The samples from this site are imbricated gneiss boulders in clast-supported channel-levee deposits on the surface of the delta. The boulders are sub- to well rounded and have smooth surfaces with relief <1 cm and scattered lichens. Briner et al. (2007) collected the samples from windswept, snow-free boulders during spring, the time of thickest snow cover in the region, so it is unlikely that the boulder surfaces experienced significant snow shielding.

4. Methods

4.1. Analytical methods

We carried out quartz separation and ^{10}Be extractions in laboratories at the University of Washington (UW), Lamont-Doherty Earth Observatory (LDEO), the University of Colorado (CU), and the University at Buffalo (UB). We separated quartz by standard methods of heavy liquid separation and repeated etching in dilute HF. We extracted ^{10}Be by adding a measured amount of Be carrier, then dissolving the sample in concentrated HF, evaporating SiF_6, and purifying Be and Al by column separation (see Stone, 2004). The Be carrier used at UW and LDEO was a low-blank carrier prepared from deep-mined beryl; that used at CU and UB was commercial Be ICP standard solution. We measured Be isotope ratios at the Lawrence Livermore National Laboratory Center for Accelerator Mass Spectrometry (LLNL-CAMS). Combined process and carrier blanks were 9800 ± 6200 atoms ^{10}Be at UW, 7500 ± 2600 atoms ^{10}Be at LDEO, $473{,}000 \pm 47{,}000$ atoms ^{10}Be at CU, and $528{,}000 \pm 68{,}000$ atoms ^{10}Be at UB. These blanks were 0.5–1.5% (UW and LDEO), 18–31% (CU), and 15–20% (UB) of the total number of ^{10}Be atoms in the samples.

Duplicate ^{10}Be measurements at the UW and LDEO labs on several samples agreed within their respective uncertainties, with one exception: UW and LDEO analyses of sample 06-NE-013-LIT disagreed at 2σ (Table 1). However, (i) we investigated this discrepancy in some detail and were unable to explain it by any systematic difference in the respective laboratory procedures; (ii) the production rate inferred from the average of the two measurements agrees with that inferred from three other samples at the Littleton Moraine, whereas production rates inferred from either of the individual measurements do not; and (iii) the ^{26}Al/^{10}Be ratio in this sample agrees with the accepted production ratio if the average of the ^{10}Be measurements is used, but disagrees if either of the individual ^{10}Be measurements are used. These observations are best explained if the difference in duplicate measurements of this sample is random and not systematic. Thus, we took the error-weighted mean of the duplicate measurements to be the best estimate of the ^{10}Be concentration for this sample as well as for the other samples that were analysed more than once.

We carried out ^{26}Al extractions at the UW lab only. We determined total Al concentrations by ICP optical emission spectrophotometry on aliquots of the dissolved quartz-HF solution. Uncertainties in total Al concentrations were 0.5–2%. We then measured Al isotope ratios at LLNL-CAMS. Total process blanks were $63{,}000 \pm 41{,}000$ atoms ^{26}Al, 0.5–2% of the total number of atoms in the sample. ^{26}Al measurements are referenced to the Al isotope ratio standards described in Nishiizumi (2004).

4.2. Note on ^{10}Be standardization

Be isotope ratios measured at LLNL-CAMS and reported in this paper were referenced to the isotope ratio standards originally described in Nishiizumi (2002). Recently, Nishiizumi et al. (2007) revised the nominal isotope ratios of those standards and, by implication, the ^{10}Be decay constant. Our measurements were made both before and after this revision. Mainly to facilitate comparison with published ^{10}Be production rate calibrations, we have renormalized the later measurements to be consistent with the original nominal values of Nishiizumi (2002). Thus, ^{10}Be concentrations and reference production rates given in this paper must be corrected if they are to be used to calculate exposure ages from recent ^{10}Be measurements referenced to the revised 2007 values of these standards. As all the calibration sites discussed here are young compared to the ^{10}Be half-life, ^{10}Be concentrations and production rates reported in this paper can be so corrected with

acceptable accuracy simply by applying a conversion factor of 0.904, the ratio of the 2007 and 2002 nominal isotope ratios for the Nishiizumi standards.

4.3. Data-reduction methods

All the calculations described here use the exposure-age calculation methods and MATLAB code used in the CRONUS-Earth online exposure age calculator, version 2.1, as described in Balco et al. (2008). For calculating ^{10}Be production rates due to muons, this uses a MATLAB implementation, described in Balco et al. (2008), of the method of Heisinger et al. (2002a,b). Production by muons is a small fraction of total ^{10}Be production (0.2 atoms g^{-1} a^{-1}) and is fully specified by this method; we are using the calibration measurements in this paper to estimate the reference ^{10}Be production rate due to spallation only. When we use 'reference ^{10}Be production rate' subsequently in this paper, we are referring to the ^{10}Be production rate by neutron spallation, referenced to sea level and high latitude. We determined best-fit reference ^{10}Be production rates applicable to the five production rate scaling schemes implemented in Balco et al. (2008) by choosing the value of the reference production rate that minimized the least-squares misfit between calculated and independently determined exposure ages for the calibration sites. Henceforth we refer to these scaling schemes by the abbreviations used in Balco et al. (2008): 'St' for that of Stone (2000) following Lal (1991); 'Du' for that of Dunai (2001); 'De' for that of Desilets et al. (2006); 'Li' for that of Lifton et al. (2005); and 'Lm' for the time-dependent adaptation of Lal (1991) implemented in Balco et al. (2008). In contrast to Balco et al. (2008), we did take account of boulder surface erosion: based on observations of surface roughness and quartz vein relief at several sites, we assumed a rock surface erosion rate of 7×10^{-5} cm a^{-1} (i.e. 1 cm in 14,000 years) and a rock density of 2.65 g cm^{-3} for all sites. We did not attempt to account for synoptic air pressure change, forest or snow cover effects, or isostatic rebound following deglaciation in calculating the reference production rates; we discuss these issues in more detail below.

5. Results

With the exception of those from the Leverett site (discussed in more detail in the next paragraph), our measurements yield reference ^{10}Be production rates significantly lower than those inferred from the global calibration data set compiled in Balco et al. (2008) (Table 2). This agrees with previous observations that the global production rate calibration data set underestimates late-glacial exposure ages in the northeastern U.S. (Balco and Schaefer, 2006; Briner et al., 2007; Rayburn et al., 2007a). Scaling schemes based on recent neutron-monitor data (the De, Du, and Li scaling schemes) come closer to reconciling our calibration data set with the global data set than schemes based on the scaling factors of Lal (1991) (the St and Lm scaling schemes). Reference production rates inferred from the regional data set are ~6% lower than those inferred from the global data set for the De, Du, and Li schemes, a difference which is commensurate with the formal uncertainties in both reference production rates of 5% and 10%, respectively. The St and Lm schemes yield reference production rates for the regional data set that are ~12% lower than those inferred from the global data set; this difference is larger relative to the formal uncertainties of 5% and 8% in these two reference production rates. The better performance of the neutron-monitor-based scaling schemes in reconciling our data with the global data set mainly reflects the difference in the elevation dependence of the production rate between the Lal (1991)-based and neutron-monitor-based scaling schemes. The elevation dependence of the production rate is larger in the neutron-monitor-based schemes, and the global data set is weighted toward mountain elevations (~2000 m), so these schemes predict lower production rates at low elevations given the same calibration data. The fact that the De, Du, and Li scaling schemes include a time-dependent magnetic field correction is relatively less important, as both calibration data sets are weighted toward high latitudes where production rates are relatively insensitive to magnetic field effects.

Two subsets of the measurements in the regional calibration data set appear to disagree with the majority of the measurements. First, the three measurements from the Leverett site yield reference production rates that are higher than those inferred from the entire data set. We sought to evaluate the importance of this by calculating reference production rates from the Leverett data and the remainder of the data set separately, and found that the best-fit reference production rate inferred from the Leverett data (5.00 ± 0.14 atoms g^{-1} a^{-1} for the St scaling scheme) does not overlap at 95% confidence with that inferred from the remainder of the data set (4.33 ± 0.21 atoms g^{-1} a^{-1}). This is not the case for any other site. In addition, the three measurements from Leverett scatter more than expected from measurement uncertainty (reduced $\chi^2 = 3.0$), whereas scatter in the remainder of the data set is commensurate with measurement uncertainty (reduced $\chi^2 = 1.1$). This suggests that the scatter in the Leverett measurements may reflect varying quantities of ^{10}Be inherited from pre-glacial exposure in addition to measurement error. Finally, the reference ^{10}Be production rate inferred from the Leverett data conflicts with minimum limits inferred from the stratigraphic relationship between the NE varve chronology and previously exposure-dated landforms in southern New England (Balco and Schaefer, 2006 and Fig. 6). For these three reasons, we excluded the Leverett data from further calculations. Second, one measurement at the Holyoke Range site also yields an apparently higher reference production rate than the remainder of the data set. However, this measurement has a relatively large uncertainty and the reference production rate inferred from it cannot be distinguished from that inferred from the remainder of the data set at 95% confidence. Thus, we retained this measurement.

Once the data from the Leverett site are excluded, the reference production rates for all the scaling schemes fit the data set to the degree expected from measurement uncertainties (reduced $\chi^2 \simeq 1$ in all cases; see Table 2. If the Leverett data are included, the reduced χ^2 values are $\simeq 3$). This provides a striking contrast with the global production rate data set in Balco et al. (2008), to which none of the scaling schemes yield statistically acceptable fits (reduced χ^2 values range between 3 and 13). The significantly better fit between all scaling schemes and the regional data set

Table 2
Best-fit reference ^{10}Be production rates from spallation with respect to various scaling schemes, inferred from the northeastern North America calibration data set. The ratio $P_{regional}/P_{global}$ is the ratio of the reference production rate determined here for the regional data set and the reference production rate inferred from the global data set by Balco et al. (2008). For samples that are young relative to the ^{10}Be half-life, this value is approximately equal to the ratio of an exposure age calculated using the global calibration data set to an exposure age for the same sample calculated using the regional calibration data set. That is, for example, an exposure age calculated using the St scaling scheme and the global calibration data set will be 12% younger than an exposure age for the same sample calculated using the same scaling scheme, but the regional calibration data set.

Scaling scheme ID[a]	Reference spallogenic ^{10}Be production rate (atoms g^{-1} a^{-1})	Reduced χ^2	Ratio $P_{regional}/P_{global}$
St	4.33 ± 0.21 (4.8%)	1.12	0.88
De	4.54 ± 0.22 (4.9%)	1.13	0.93
Du	4.57 ± 0.23 (4.9%)	1.11	0.94
Li	4.95 ± 0.24 (4.9%)	1.20	0.92
Lm	4.26 ± 0.21 (4.9%)	1.10	0.88

[a] Follows Balco et al. (2008). See text for details.

mainly reflects the fact that the regional data set covers only a small range of elevation and geomagnetic cutoff rigidity, and is thus relatively insensitive to scaling assumptions.

We measured ^{26}Al concentrations in only five samples. In agreement with expectations, all of these samples had ^{26}Al/^{10}Be ratios indistinguishable from the commonly accepted production ratio of 6.1 (this value reflects ^{10}Be concentrations normalized to the ^{10}Be standards of Nishiizumi (2002); if the revised standards of Nishiizumi et al. (2007) are used, the corresponding value of the ^{26}Al/^{10}Be production ratio is 6.75). Thus, we have not made a separate calibration of ^{26}Al production rates in this study. As also suggested in similar studies (Balco et al., 2008), one can determine reference ^{26}Al production rates consistent with the regional calibration data set by multiplying the ^{10}Be production rates given in Table 2 by the production ratio.

6. Discussion

6.1. Why do production rates in northeast North America disagree with the global calibration data set?

There are several possible causes of the discrepancy between reference ^{10}Be production rates inferred from this regional data set and from the global data set. First of all, it is possible that the better performance of the De, Du, and Li scaling schemes in reconciling the two data sets provides supporting evidence for the larger elevation dependence of nuclide production rates in neutron-monitor-based scaling schemes relative to the St and Lm scaling schemes. In this case, we might argue that the reference production rates inferred from the two data sets actually agree within error when the De, Du, and Li scaling schemes are used, and this agreement provides evidence that the neutron-monitor-based scaling schemes better depict the true elevation dependence of the production rate than the Lal (1991)-based schemes. However, the global calibration data set does not support this argument (Fig. 4). When any available scaling scheme is fit to the global calibration data set, there remains an elevation-dependent residual, which is larger for neutron-monitor-based scaling schemes, in the differences between calculated and independently determined exposure ages of the calibration sites. That is, in the global data set, higher-elevation calibration sites yield relatively low reference production rates, suggesting that the neutron-monitor-based scaling schemes overcorrect for elevation (Fig. 4 and Balco et al., 2008). In contrast, the regional calibration data set does not fit this trend. The observation that reference production rates inferred from low-elevation sites in the regional data set are lower than reference production rates inferred from higher-elevation sites in the global data set suggests the opposite, that all scaling schemes undercorrect for elevation differences. This inconsistency makes it impossible to interpret our results as favoring a larger elevation dependence of the production rate given the currently available data. In addition, the regional data set spans too small an elevation range to provide any leverage on the elevation dependence of the production rate by itself.

Second, it is possible that the fact that we did not account for shielding by forest or snow cover caused us to underestimate the true ^{10}Be production rates at our sites. It is unlikely that this effect could produce a systematic difference between production rates inferred from this data set and the global data set, because many measurements in the global calibration data set are also located in forested or seasonally snow-covered regions, but were not corrected for these effects. Furthermore, neither effect is large enough to explain the difference in production rates derived from the two data sets. At the Baffin Island site, as noted above, we sought to exclude the possibility of snow shielding entirely by collecting samples from snow-free boulders in early spring, the time of maximum snow cover. For the New England sites, we estimated the effect of snow shielding using historical snow depth measurements from nearby meteorological stations. We obtained long-term daily snow depth measurements from stations at Bethlehem, NH (near the Littleton Moraine sample sites), Hanover, NH (near the upper Connecticut River Valley sites), and Dannemora, NY (near the Cobblestone Hill sites) from the U.S. Historical Climatology Data Network (Williams et al., 2007). The records from these stations spanned the years 1948–1991, 1926–2005, and 1926–2005, respectively. They include daily snow depth and liquid precipitation amounts, but not snow density or snow water equivalent. As we require the snow water equivalent to calculate shielding, we used a linear positive degree day model (e.g. Patterson, 1994) to estimate daily melt rates. For each period of snow cover, we obtained the proportionality factor between positive degree days and melt by equating total liquid precipitation and total positive degree days during that period. Integrating daily liquid precipitation less inferred melt through each period of snow cover thus yielded an estimate of daily snow water equivalent. We could then

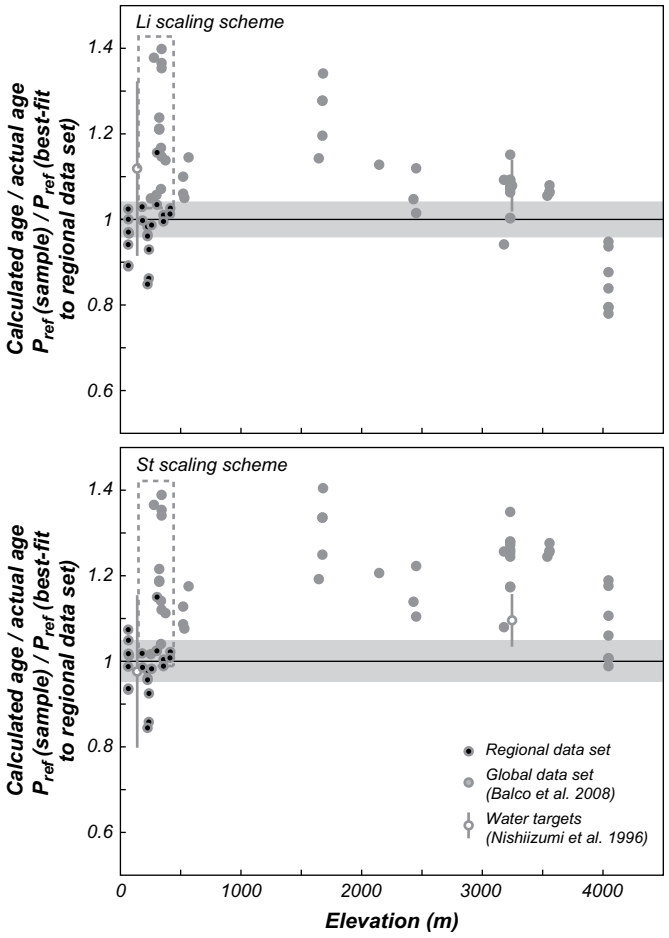

Fig. 4. Comparison between our regional calibration data set and the global calibration data set from Balco et al. (2008). As in Fig. 3, (i) each data point shows the ratio of the exposure age calculated from a ^{10}Be measurement at a calibration site, using the reference production rate inferred from the our regional calibration data set, to the independently determined exposure age of the site, and (ii) the gray band reflects the 1σ uncertainty in the reference production rate inferred from the regional data set. The black circles are the regional calibration data set shown in Fig. 3, with the Leverett data excluded. The gray circles are the global calibration data set from Balco et al. (2008). We have omitted error bars from these two data sets for readability; they are shown in Fig. 3 in this paper and Fig. 5 of Balco et al. (2008). The open circles with error bars represent production rates inferred from water target experiments by Nishiizumi et al. (1996). The dashed box highlights data from the New Jersey calibration site of Larsen (1996) (see text for discussion).

calculate the annually averaged snow water equivalent, and thus the overall shielding effect, at each station. We found that annually averaged snow water equivalents at Bethlehem, Hanover, and Dannemora were 2.1 cm, 1.3 cm, and 1.7 cm, respectively. This would reduce the ^{10}Be production rate at these stations by 0.7%, 0.4%, and 0.5%. As the average snow depth on boulder surfaces is likely less than on open, flat ground due to wind and solar heating effects, these values probably overestimate the true snow shielding at our sample sites. Even given the possibility of increased snow depths immediately after deglaciation, therefore, snow shielding at these sites is an order of magnitude less than required to explain the discrepancy between reference production rates inferred from the regional and global data sets. With regard to forest cover, the Baffin Island site is not, and has not been, forested; the Cobblestone Hill site is located in a sparsely forested pine barren, and the remainder of the sites is located in boreal to temperate spruce-fir and hardwood forests. Although no comparative measurements of the cosmic-ray flux above and beneath forest cover exist, Plug et al. (2006) estimated the cosmic-ray shielding effects of forest cover using a highly simplified particle transport model. For similar forests to those present at our sites in central New England, they estimated that the forest cover would reduce boulder surface production rates by 2.5%. This amount is much less than required to explain the difference between production rates inferred from the regional and global calibration data sets, especially in light of the fact that this correction has not been made for forested sites in the global calibration data set. In addition, we can in principle evaluate the importance of forest cover in our data set by observing that the differences in forest type among our sites should result in systematic scatter in production rates inferred from those sites: sites with thin forest cover (Baffin Island and Cobblestone Hill) should yield systematically higher reference production rates than forested sites. We observe no such relationship; however, the expected magnitude of this effect is similar to both measurement uncertainty and differences among scaling schemes, so this observation does not provide strong constraints on the importance of forest shielding.

Third, as the production rate calculations in Balco et al. (2008) are based on the modern atmospheric pressure distribution, it is possible that long-term synoptic atmospheric pressure changes could contribute to the failure of production rate scaling schemes to reconcile these data with the global data set. If atmospheric pressure at the sites had been higher in the past, production rates would be lower, and we would underestimate the production rate at the present atmospheric pressure if we did not take this into account. However, Staiger et al. (2007) considered this and showed that, in fact, atmospheric pressure was most likely lower at ice-marginal sites during deglaciation due to katabatic wind effects. Thus, it is unlikely that time-dependent atmospheric pressure changes have caused us to underestimate reference production rates. However, Staiger et al. (2007) also pointed out that atmospheric compression associated with the generally colder climate during the last glacial maximum would have disproportionately decreased atmospheric pressure, and thus increased production rates, at high-elevation sites relative to low-elevation sites. Therefore, not accounting for atmospheric compression could cause a spurious elevation dependence in production rates inferred from late-glacial-aged calibration sites, with the correct sense as the observed difference between the regional and global data sets. However, (i) Staiger et al. (2007) found that this effect was relatively small (order 1% of the reference production rate), and (ii) this effect also fails to explain the elevation-dependent residuals of opposite sense in the global calibration data set.

Finally, our calibration sites are located in ice-marginal environments and were therefore affected by glacioisostatic elevation changes. Even if the mean atmospheric pressure distribution relative to present sea level did not change over time at our sites, at the time they were first exposed by ice retreat, they were at a lower elevation due to isostatic depression. They were therefore located deeper in the atmosphere and would have experienced lower production rates. If we did not account for this effect, we could systematically underestimate production rates. We attempted to evaluate the importance of this effect by extracting elevation change histories for the Littleton, Cobblestone Hill, and Clyde River sites from the ICE-5 G glacioisostatic rebound model (Peltier, 2004), and computing production rate histories therefrom. We found that, if the present atmospheric pressure distribution were held constant, isostatic rebound effects would cause us to underestimate the production rate at these sites by 1.5%, 2.5%, and 2.5%, respectively. This effect would be counteracted to an unknown extent by katabatic wind effects on the air pressure distribution as discussed above, so the true underestimate of the production rate must be less than these values. As only a minority of calibration sites in the global data set are located marginal to large ice sheets, this effect could produce a small systematic offset with the correct sense between reference production rates inferred from the ice-marginal sites in this data set and those inferred from the global data set. However, it is too small to explain the observed mismatch.

To summarize, although we did not correct for snow cover, time-dependent changes in atmospheric pressure, or isostatic rebound in inferring reference production rates from the regional data set, these potential corrections, even taken together, are significantly smaller than the observed mismatch between the regional and global data sets (ca. 2–3% vs. 6–12%). Furthermore, Balco et al. (2008) did not apply similar corrections consistently to the global data set either, which further reduces the potential of these corrections to explain the mismatch.

Completeness requires that we discuss one final issue raised by the comparison between the regional and global calibration data sets. The global data set includes ^{10}Be measurements from sites near the terminal moraine of the Laurentide Ice Sheet in New Jersey (Larsen, 1996), which is relatively close to our calibration sites in New England (Fig. 4). Given the independent chronology proposed by Larsen (1996), these measurements yield reference ^{10}Be production rates that are higher than predicted by our regional data set. With the St scaling scheme, for example, these data yield reference ^{10}Be production rates widely scattered between 4.4 and 6.1 atoms g^{-1} a^{-1}, around an average of 5.2 ± 0.6 atoms g^{-1} a^{-1}. However, only the minimum possible exposure age of these sites is well constrained by radiocarbon dates on postglacial sediments (Larsen, 1996; Clark et al., 1995; Cotter, 1984). There are no direct maximum limiting radiocarbon dates on terminal moraine deposits near these sites, and these authors inferred the maximum possible exposure age of their sites by long-distance correlation to radiocarbon dates below presumed correlative deposits from southeastern New England and the offshore continental shelf (e.g. Stone and Borns, 1986). These radiocarbon dates have since been superseded by exposure ages that, regardless of the scaling scheme or calibration data set used, suggest an older age for the terminal moraine complex (Balco et al., 2002; Balco and Schaefer, 2006). Thus, we suggest that the calibration measurements of Larsen (1996) are best interpreted as maximum limits on ^{10}Be production rates. In this case, their measurements would be consistent with the reference production rates we infer from our regional calibration data set, and would suggest a deglaciation age for the terminal moraine in New Jersey near 25 ka.

6.2. The regional calibration data set should be used for northeastern North America

The discussion above indicates that there is no obvious explanation for the discrepancy between reference production rates

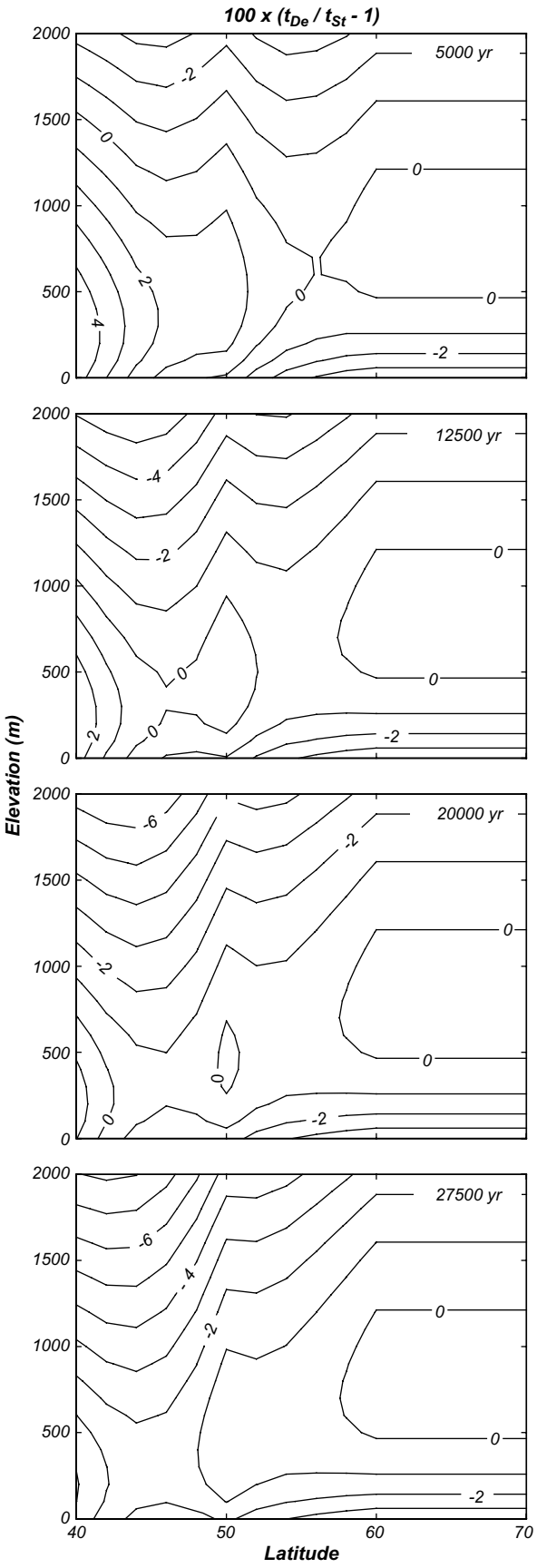

inferred from the regional and global calibration data sets, and we are unable to propose any simple correction scheme that would reconcile the two. We conclude that the global calibration data set, used with any available scaling scheme, will produce inaccurate exposure ages for late-glacial landforms in northeastern North America. The regional data set should be used for this purpose instead. All commonly used scaling schemes fit the regional calibration data set within measurement error, which indicates that scaling scheme uncertainties are negligible within the range of locations and ages spanned by the calibration sites. Thus, exposure ages for sites that are similar in location and age to our calibration sites, if calculated using production rates and uncertainties in Table 2, will be consistent with calibrated radiocarbon dates within the uncertainty of the exposure age. In general, this is not true for exposure ages calculated using the global data set. In addition, the uncertainty in the reference production rate inferred from the regional data set (~5%) is significantly smaller than that inferred from the global data set (~10%), so using the regional calibration data set improves both the accuracy and the precision of the resulting exposure ages. This, in turn, improves confidence in correlating exposure age and calibrated radiocarbon chronologies for late-glacial events in northeastern North America.

6.3. For what region of locations and ages will the regional calibration data set yield accurate results?

The reason that all scaling schemes fit the regional data set equally well is that this data set spans a relatively small range of age, elevation, and geomagnetic cutoff rigidity, so scaling corrections between the sites are small. This restriction has the disadvantage that the regional data set is not useful for comparative evaluation of different scaling schemes. On the other hand, it has the advantage that if we use the regional calibration data set to calculate exposure ages at sites that are similar in age and location to the calibration data, the accuracy of the exposure ages is minimally affected by differences in scaling assumptions between different scaling schemes.

We can get an idea of how far we can extrapolate away from the calibration data set in age and location while still maintaining accuracy by looking at the geographic and temporal divergence between exposure ages calculated with the regional production rate data set, but different scaling schemes. Fig. 5 shows an example. As the effect of magnetic field changes is minimized at the relatively high-latitude region that we are interested in here, the main scaling assumption that we are concerned about is the uncertainty in the elevation dependence of the production rate, which is manifested in the large divergence with elevation of the scaling schemes based on neutron-monitor measurements and those based on the Lal (1991) scaling factors. As our calibration data are located at elevations <500 m, these two groups of scaling schemes begin to diverge at higher elevations (see Fig. 5. A smaller divergence of opposite sense that appears at very low elevation and latitude > 55° is an artifact that arises from the fact that the scaling

Fig. 5. Difference between exposure ages for sites at high northern latitudes calculated using our regional calibration data set, but different scaling schemes. The plots show contours of the percentage difference between an exposure age calculated using the scaling scheme of Desilets et al. (2006) and an exposure age calculated from the same ^{10}Be concentration, but with the scaling scheme of Stone (2000). A contour with a value of 2, for example, indicates that the exposure age calculated with the Desilets et al. (2006) scaling scheme is 2% older than the exposure age calculated according to Stone (2000). This comparison exemplifies differences between scaling schemes based on neutron-monitor data (De, Du, Li) and those based on the scaling of Lal (1991) (St, Lm). All three neutron-monitor scaling schemes yield similar results. The four panels are calculated for exposure times of 5000, 12,500, 20,000, and 27,500 years. These plots are drawn for 75 °W longitude. The scaling schemes are implemented as described in Balco et al. (2008).

factors of Lal (1991) are represented by polynomial functions and those of other authors are represented by exponential functions). In addition, the difference between time-independent and time-dependent scaling schemes becomes important at lower latitudes where paleomagnetic field effects become important. Again because paleomagnetic field effects are relatively small at the latitudes of interest here, the divergence among scaling schemes does not depend strongly on age during the age range of interest for deglaciation in northeastern North America (ca. 25–7.5 ka) (Fig. 5).

The fact that magnetic field effects are small at relatively high latitudes suggests that reference production rates derived from our regional calibration data set for northeastern North America should in principle also yield accurate exposure ages at high latitude, low elevation sites elsewhere. As exposure ages from glacial landforms at middle to high latitudes worldwide are commonly cited to support or contradict hypotheses about the interhemispheric correlation of late-glacial climate events (e.g. Schaefer et al., 2006), this is an important issue: geographically systematic errors in production rate estimates could produce spurious such correlations, or obscure real ones. At first order, production rate scaling schemes predict that production rate variations at high latitudes should be (i) nearly invariant with longitude, and (ii) nearly symmetric about the equator. In detail, however, this conclusion depends on the magnetic field reconstruction incorporated in the scaling scheme. For example, Lifton et al. (2008) pointed out that failure to account for non-dipole components of the magnetic field could result in systematic longitudinal variations as well as interhemispheric differences in production rate estimates for latitudes up to ~50°. Thus, extrapolating reference production rates based on our regional calibration data set to regions that are at similar latitude and elevation, but are far away relative to the wavelength of magnetic field variations, could result in inaccurate production rate estimates for those regions. There are few data available to evaluate this possibility. The global calibration data set includes only one site at low elevation in northern Europe, that of Stone et al. (1998) from western Scotland, which yields reference production rates several percent higher than inferred from our regional calibration data set.

In addition, there is another important difference between applying our calibration data set to late-glacial ice-marginal landforms in northeastern North America alone and applying it worldwide. Ice-marginal sites in northeastern North America experienced significant atmospheric pressure changes and isostatic rebound during deglaciation. We do not suggest explicitly accounting for these processes in using the reference production rates calculated here to calculate exposure ages for ice-marginal landforms in northeastern North America, because: (i) we cannot reconstruct the combined effect of these changes on production rates precisely, and (ii) the fact that the calibration sites are also ice-marginal landforms that experienced the same changes minimizes the importance of this uncertainty in relating exposure ages of calibration sites and unknown-age sites. However, extending the reference production rates determined here to other regions without accounting for these effects could produce additional systematic errors.

To summarize, we suggest that the regional calibration data set will yield accurate exposure ages – that is, exposure ages that agree with the calibrated radiocarbon time scale within their uncertainties – for ice-marginal deposits in eastern North America north of ~40 °N latitude and below ~1000 m elevation, throughout deglaciation. There are not enough data from other regions available to evaluate whether or not the regional calibration data set will yield similarly accurate exposure ages at low-latitude, low-elevation sites worldwide. We emphasize that improving the global performance of production rate scaling methods is not the purpose of this work: our goals are only to: (i) show that using a regional calibration data set for late-glacial landforms in northeastern North America minimizes production rate scaling uncertainties and successfully reconciles exposure age and radiocarbon deglaciation chronologies, and (ii) present this strategy as a guide for other regional studies.

6.4. Example recalculation of existing exposure ages

The discussion above implies that previously published exposure ages from sites in northeastern North America should be recalculated using the regional calibration data set. As an example, we carry

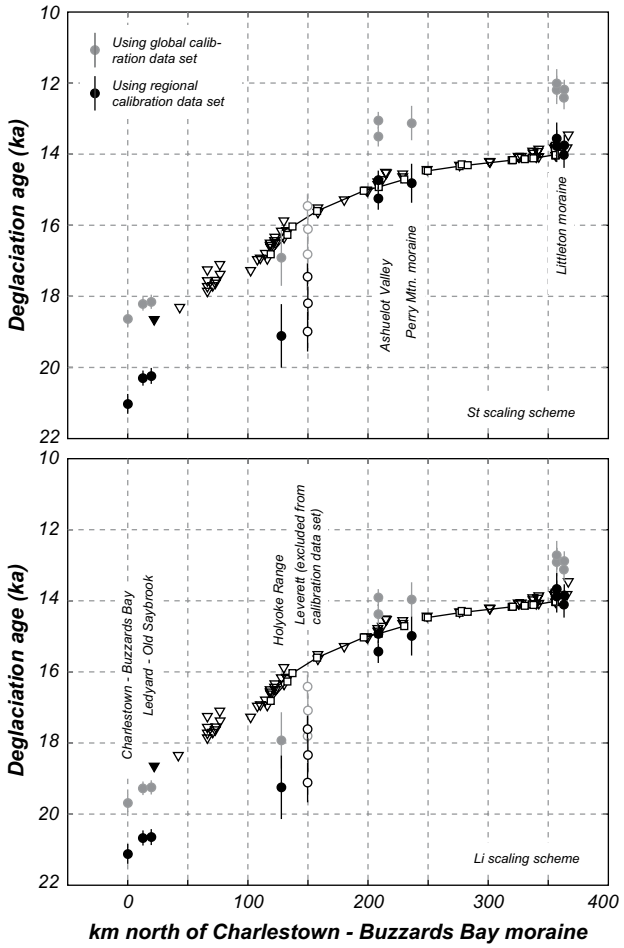

Fig. 6. Time-distance diagrams for ice recession through central New England. The line of projection is indicated in Fig. 1. Open symbols show the deglaciation chronology inferred from the New England varve chronology, fixed to the calibrated radiocarbon time scale as described in the text: the open squares connected by the black line represent basal or ice-proximal varves that closely indicate the position of the ice margin in a particular varve year; the open triangles are younger limiting ages where the bottom of a varve section is not exposed. The black triangle shows a calibrated radiocarbon date from basal peat, located immediately ice-proximal to the Ledyard moraine, that provides a minimum limiting age for this moraine (McWeeney, 1995). The closed circles are exposure ages from this study, Balco and Schaefer (2006), and Balco et al. (2002): the gray circles are exposure ages calculated using the global calibration data set, the black circles are exposure ages calculated using the regional calibration data set described here, and the vertical lines represent 1σ measurement uncertainties. The uncertainties for the Ledyard, Old Saybrook, and Charlestown-Buzzards Bay moraines reflect the error-weighted mean of 7, 7, and 10 ^{10}Be measurements, respectively (see Balco and Schaefer (2006) and Balco et al. (2002) for details). When using the regional calibration data set, we are in effect forcing the varve and exposure-age deglaciation chronologies in the northern Connecticut River Valley to agree, which changes the exposure-age chronology for southern New England as well. The main points of this figure are that (i) the regional and global calibration data sets yield significantly different exposure ages for the southern New England moraines, and (ii) using the regional data set nearly eliminates the dependence of the inferred age of these moraines on the choice of production rate scaling scheme. In addition, this figure highlights the disagreement between the Leverett exposure ages and the rest of the data set: if the production rate was adjusted to make the exposure ages at Leverett agree with the varve chronology, exposure ages in southern New England would become impermissibly young.

out this exercise for previously published exposure ages from south-central New England. Fig. 6 compares varve, radiocarbon, and exposure-age chronologies for central New England, including exposure ages for sites in the upper Connecticut River Valley from this work, exposure ages for the Ledyard and Old Saybrook moraines in southeastern Connecticut from Balco and Schaefer (2006), and exposure ages for the Buzzards Bay moraine from Balco et al. (2002). All production rate scaling schemes, when calibrated using the global calibration data set, result in deglaciation ages for both southern New England and upper Connecticut River Valley sites that are significantly younger than deglaciation ages inferred from the varve chronology as well as minimum limiting radiocarbon dates from basal organic sediment. Using the regional calibration data set instead results in: (a) exposure ages for the upper Connecticut River Valley that agree with the varve chronology, and (b) exposure ages for southern New England that are consistent with minimum limiting ages from the varve chronology and basal radiocarbon ages. This is true for all scaling schemes; we have shown results for the St and Li scaling schemes in Fig. 6 as representative examples. It is no surprise that (a) above is true – because these sites are incorporated in the calibration data set – but (b) represents a significant improvement in the accuracy of exposure ages for ice-marginal landforms in southern New England. In previous work, we were only able to show that the global calibration data set yielded incorrect ages for these moraines. The regional production rate calibration data set both enables us to determine the correct age of these moraines, thus permitting correlation with glacial and climate events elsewhere, and provides a quantitative estimate of the uncertainty of this age relative to other dating techniques.

Recalculating the exposure ages for the Ledyard, Old Saybrook, and Buzzards Bay moraines, using the St scaling scheme and the regional calibration data set, indicates that these moraines were emplaced 20.2 ± 1.0 ka, 20.3 ± 1.0 ka, and 21.0 ± 1.0 ka, respectively. These uncertainties reflect error-weighted averages of 7, 7, and 10 measurements, respectively, and include the production rate uncertainty from Table 2. Thus, these ages can be directly compared with other deglaciation chronologies based on calibrated radiocarbon, varve, or ice core timescales. These moraines are significantly older than we suggested in previous work; we will discuss the significance of the revised ages in a subsequent paper.

7. Conclusions

Existing production rate scaling methods fail to reconcile ^{10}Be production rate measurements in northeastern North America with the commonly used global production rate data set. We suggest that the local calibration data set should be used for calculating the exposure age of late-glacial deposits in this region. This approach minimizes, if not eliminates, systematic differences between radiocarbon and exposure-age deglaciation chronologies in northeastern North America, thus improving confidence in correlating late-glacial events with coeval climate changes.

Acknowledgements

GB was supported by a fellowship from the National Science Foundation, Office of Polar Programs during the period of this work. JMS thanks Roseanne Schwartz for help with the sample preparation and acknowledges support from the Comer Science and Educational Foundation, the Lamont summer-intern program and the Lamont Climate Center. This is Lamont-Doherty Earth Observatory Contribution 7195. RCF's participation was partially supported by the U.S. Department of Energy under contract no. DE-AC52-07NA27344. Some AMS measurements were supported by the CRONUS-Earth project (NSF grant EAR-0345949). We thank Woody Thompson for his help in identifying the Littleton Moraine sites, and David Franzi for help with the Cobblestone Hill sites.

Editorial handling by: J.C. Gosse

References

Antevs, E., 1922. The Recession of the Last Ice Sheet in New England: Research Series No. 11. American Geographical Society.
Antevs, E., 1928. The Last Glaciation with Special Reference to the Ice Sheet in North America: Research Series No. 17. American Geographical Society.
Balco, G., Schaefer, J., 2006. Cosmogenic-nuclide and varve chronologies for the deglaciation of southern New England. Quaternary Geochronology 1, 15–28.
Balco, G., Stone, J., Lifton, N., Dunai, T., 2008. A complete and easily accessible means of calculating surface exposure ages or erosion rates from ^{10}Be and ^{26}Al measurements. Quaternary Geochronology.
Balco, G., Stone, J., Porter, S., Caffee, M., 2002. Cosmogenic-nuclide ages for New England coastal moraines, Martha's Vineyard and Cape Cod, Massachusetts, USA. Quaternary Science Reviews 21, 2127–2135.
Borns, H., Doner, L., Dorion, C., Jacobson, G., Kaplan, M., Kreutz, K., Lowell, T., Thompson, W., Wedde, T.K., 2004. The deglaciation of Maine, USA. In: Ehlers, J., Gibbard, P. (Eds.), Quaternary Glaciations – Extent and Chronology, Volume 2, Part II. Elsevier, pp. 89–110.
Briner, J., Overeem, I., Miller, G., Finkel, R., 2007. The deglaciation of Clyde Inlet, northeastern Baffin Island, Arctic Canada. Journal of Quaternary Science 22, 223–232.
Broecker, W., 2006. Was the Younger Dryas triggered by a flood? Science 312, 1146–1148.
Clark, D., Bierman, P., Larsen, P., 1995. Improving *in-situ* cosmogenic chronometers. Quaternary Research 44, 367–377.
Cotter, J., 1984. The Minimum Age of the Woodfordian Deglaciation of Northeastern Pennsylvania and Northwestern New Jersey. Ph.D. thesis, Lehigh University.
Desilets, D., Zreda, M., Prabu, T., 2006. Extended scaling factors for in situ cosmogenic nuclides: new measurements at low latitude. Earth and Planetary Science Letters 246, 265–276.
Dunai, T., 2001. Influence of secular variation of the magnetic field on production rates of in situ produced cosmogenic nuclides. Earth and Planetary Science Letters 193, 197–212.
Dyke, A., Moore, A., Robertson, L., 2003. Deglaciation of North America. Geological Survey of Canada, Open-File Report 1574. Geological Survey of Canada.
Franzi, D., Rayburn, J., Knuepfer, P., Cronin, T., 2007. Late Quaternary history of Northeastern New York and adjacent parts of Vermont and Quebec: Guidebook to the 70th annual reunion of the Northeast Friends of the Pleistocene.
Franzi, D., Rayburn, J., Yansa, C., Knuepfer, P., 2002. Late glacial water bodies in the Champlain and St. Lawrence lowlands and their paleoclimatic implications. In: McLelland, J., Karabinos, P. (Eds.), Guidebook for Fieldtrips in New York and Vermont: New England Intercollegiate Geological Conference 94th Annual meeting and New York State Geological Association 74th Annual meeting, pp. A5–1–A5–23.
Frost, R., 1915. Mending wall. In: North of Boston. David Nutt and Company.
Heisinger, B., Lal, D., Jull, A.J.T., Kubik, P., Ivy-Ochs, S., Knie, K., Nolte, E., 2002a. Production of selected cosmogenic radionuclides by muons: 2. Capture of negative muons. Earth and Planetary Science Letters 200 (3–4), 357–369.
Heisinger, B., Lal, D., Jull, A.J.T., Kubik, P., Ivy-Ochs, S., Neumaier, S., Knie, K., Lazarev, V., Nolte, E., 2002b. Production of selected cosmogenic radionuclides by muons 1. Fast muons. Earth and Planetary Science Letters 200 (3–4), 345–355.
Lal, D., 1991. Cosmic ray labeling of erosion surfaces: in situ nuclide production rates and erosion models. Earth and Planetary Science Letters 104, 424–439.
Larsen, P., 1996. In-situ Production Rates of Cosmogenic ^{10}Be and ^{26}Al Over the Past 21,500 Years Determined from the Terminal Moraine of the Laurentide Ice Sheet, North-central New Jersey. Ph.D. thesis, University of Vermont.
Lifton, N., Bieber, J., Clem, J., Duldig, M., Evenson, P., Humble, J., Pyle, R., 2005. Addressing solar modulation and long-term uncertainties in scaling secondary cosmic rays for in situ cosmogenic nuclide applications. Earth and Planetary Science Letters 239, 140–161.
Lifton, N., Smart, D., Shea, M., 2008. Scaling time-integrated in situ cosmogenic nuclide production rates using a continuous geomagnetic model. Earth and Planetary Science Letters 268, 190–201.
Lougee, R., 1935. Time measurements of an ice readvance at Littleton, NH. Proceedings of the National Academy of Sciences 21, 36–41.
Lowell, T., Fisher, T., Comer, G., Hajdas, I., Waterson, N., Glover, K., Loope, H., Schaefer, J., Rinterknecht, V., Broecker, W., Denton, G., Teller, J., 2005. Testing the Lake Agassiz meltwater trigger for the Younger Dryas. EOS, Transactions, American Geophysical Union 86, 365–373.
Lowell, T., Hayward, R., Denton, G., 1999. Role of climate oscillations in determining ice-margin position: hypothesis, examples, and implications. In: Mickelson, D., Attig, J. (Eds.), Glacial Processes Past and Present: Geological Society of America Special Paper 337. Geological Society of America, Boulder, CO, pp. 193–203.
Mattox, R., 1951. Surficial Geologic Map of the Mount Toby Quadrangle, Massachusetts. U.S. Geological Survey.
McWeeney, L.J., 1995. Revised vegetation history for the post-glacial period (15,200–10,000 ^{14}C years B.P.) in southern New England. Geological Society of America Abstracts with Programs 27, 68.
Muscheler, R., Kromer, B., Björck, S., Svensson, A., Friedrich, M., Kaiser, K., Southon, J., 2008. Tree rings and ice cores reveal ^{14}C calibration uncertainties during the Younger Dryas. Nature Geoscience 1, 263–267.

Nishiizumi, K., 2002. ^{10}Be, ^{26}Al, ^{36}Cl, and ^{41}Ca AMS standards: Abstract O16-1. In: 9th Conference on Accelerator Mass Spectrometry. p. 130.
Nishiizumi, K., 2004. Preparation of ^{26}Al AMS standards. Nuclear Instruments and Methods in Physics Research B 223–224, 388–392.
Nishiizumi, K., Finkel, R., Klein, J., Kohl, C., 1996. Cosmogenic production of ^{7}Be and ^{10}Be in water targets. Journal of Geophysical Research 101 (B10), 22,225–22,232.
Nishiizumi, K., Imamura, M., Caffee, M., Southon, J., Finkel, R., McAnich, J., 2007. Absolute calibration of ^{10}Be AMS standards. Nuclear Instruments and Methods in Physics Research B 258, 403–413.
Patterson, W., 1994. The Physics of Glaciers, third ed. Pergamon Press.
Peltier, W., 2004. Global glacial isostasy and the surface of the ice-age Earth: the ICE-5G model and GRACE. Annual reviews of earth and planetary science 32, 111–149.
Plug, L., Gosse, J., McIntosh, J., Bigley, R., 2006. Attenuation of cosmic ray flux in temperate forest. Journal of Geophysical Research 112 F02022.
Rayburn, J., Briner, J., Franzi, D., 2007a. Cosmogenic exposure dating of an ice-marginal flood scour and boulder bar near the New York–Quebec border. Abstracts with programs, Geological Society of America Northeastern Section, 42nd Annual Meeting.
Rayburn, J., Franzi, D., Knuepfer, P., 2007b. Evidence from the Lake Champlain Valley for a later onset of the Champlain Sea, and implications for late glacial meltwater routing to the North Atlantic. Palaeogeography, Palaeoclimatology, Palaeoecology 246, 62–74.
Rayburn, J., Franzi, D., Knuepfer, P., 2008. A record of meltwater flood discharges in glacial Lake Vermont sediments from the Lake Champlain Valley. Abstracts with programs, Geological Society of America Northeastern Section, 43rd Annual Meeting.
Rayburn, J., Knuepfer, P., Franzi, D., 2005. A series of large late Wisconsinan meltwater floods through the Champlain and Hudson Valleys, New York State, USA. Quaternary Science Reviews 24, 2410–2419.
Reimer, P., Baillie, M., Bard, E., Bayliss, A., Beck, J., Bertrand, C., Blackwell, P., Buck, C., Burr, G., Cutler, K., Damon, P., Edwards, R., Fairbanks, R., Friedrich, M., Guilderson, T., Hogg, A., Hughen, K., Kromer, B., McCormac, G., Manning, S., Ramsey, C., Reimer, R., Remmele, S., Southon, J., Stuiver, M., Talamo, S., Taylor, F., van der Plicht, J., Weyhenmeyer, C., 2004. INTCAL04 terrestrial radiocarbon age calibration, 0–26 cal kyr bp. Radiocarbon 46, 1029–1058.
Richard, P., Occhietti, S., 2005. ^{14}C chronology for ice retreat and inception of Champlain Sea in the St. Lawrence lowlands. Quaternary Research 63, 353–358.
Ridge, J., 2001. Surficial geologic map of part of the Claremont and Springfield 7.5-minute quadrangles (7.5 × 15 minutes), Vermont-New Hampshire: Open-File Report Geo-164. 3 map sheets, scale 1:24,000. New Hampshire State Geological Survey.
Ridge, J., 2003. The last deglaciation of the northeastern United States: a combined varve, paleomagnetic, and calibrated ^{14}C chronology. In: Cremeens, D., Hart, J. (Eds.), Geoarchaeology of Landscapes in the Glaciated Northeast: New York State Museum Bulletin 497. University of the State of New York, Albany, NY, pp. 15–45.
Ridge, J., 2004. The Quaternary glaciation of western New England with correlations to surrounding areas. In: Ehlers, J., Gibbard, P. (Eds.), Quaternary Glaciations – Extent and Chronology. Elsevier, pp. 169–199.
Ridge, J., 2008. North American Glacial Varve Project Available from: http://ase.tufts.edu/geology/varves/.
Ridge, J., Besonen, M., Brochu, M., Brown, S., Callahan, J., Cook, G., Nicholson, R., Toll, N., 1999. Varve, paleomagnetic, and ^{14}C chronologies for late Pleistocene events in New Hampshire and Vermont (U.S.A.). Géographie Physique et Quaternaire 53, 79–106.
Ridge, J., Canwell, B., Kelly, M., Kelley, S., 2001. Atmospheric ^{14}C chronology for late Wisconsinan deglaciation and sea-level change in eastern New England using varve and paleomagnetic records. In: Weddle, T., Retelle, M. (Eds.), Deglacial History and Relative Sea-level Changes, Northern New England and Adjacent Canada, Geological Society of America Special Paper 351, pp. 173–191.
Ridge, J., Larsen, F., 1990. Reevaluation of Antevs' New England varve chronology and new radiocarbon dates of sediments from glacial Lake Hitchcock. Geological Society of America Bulletin 102, 889–899.
Ridge, J., Thompson, W., Brochu, M., Brown, S., Fowler, B., 1996. Glacial geology of the upper Connecticut Valley in the vicinity of the lower Ammonusuc and Passumpsic Valleys of New Hampshire and Vermont. In: Van Baalen, M. (Ed.), Guidebook to Field Trips in Northern New Hampshire and Adjacent Regions of Maine and Vermont: New England Intercollegiate Geologic Conference, 88th Annual Meeting, pp. 309–340.
Ridge, J., Toll, N., 1999. Are late-glacial climate oscillations recorded in varves of the upper Connecticut Valley, northeastern United States? Geologiska Foreningens i Stockholm Förhandlingar 121, 187–193.
Rittenour, T., 1999. Drainage History of Glacial Lake Hitchcock, Northeastern USA. Master's thesis, University of Massachusetts, Amherst.
Rittenour, T., Brigham-Grette, J., Mann, M., 2000. El Niño-like climate teleconnections in New England during the late Pleistocene. Science 288, 1039–1042.
Schaefer, J., Denton, G., Barrell, D., Ivy-Ochs, S., Kubik, P., Andersen, B., Phillips, F., Lowell, T., Schlücter, C., 2006. Near-synchronous interhemispheric termination of the Last Glacial Maximum in mid-latitudes. Science 312, 1510–1513.
Staiger, J., Gosse, J., Toracinta, R., Oglesby, B., Fastook, J., Johnson, J., 2007. Atmospheric scaling of cosmogenic nuclide production: climate effect. Journal of Geophysical Research 112, BO2205.
Stone, B., Borns, H., 1986. Pleistocene glacial and interglacial stratigraphy of New England, Long Island, and adjacent Georges Bank and Gulf of Maine. In: Sibrava, V., Bowen, D., Richmond, G. (Eds.), Quaternary Glaciations in the Northern Hemisphere: Quaternary Science Reviews Volume 5. Pergamon Press, Oxford, pp. 39–52.
Stone, J., 2004. Extraction of Al and Be from Quartz for Isotopic Analysis UW Cosmogenic Nuclide Lab Methods and Procedures. Available from: http://depts.washington.edu/cosmolab/chem.html.
Stone, J., Ballantyne, C., Fifield, L., 1998. Exposure dating and validation of periglacial weathering limits, northwest Scotland. Geology 26, 587–590.
Stone, J.O., 2000. Air pressure and cosmogenic isotope production. Journal of Geophysical Research 105 (B10), 23753–23759.
Thompson, W., Fowler, B., Dorion, C., 1999. Deglaciation of the northwestern White Mountains, New Hampshire. Geographie physique et Quaternaire 53, 59–77.
Thompson, W., Fowler, B., Flanagan, S., Dorion, C., 1996. Recession of the late Wisconsinan ice sheet from the northwestern White Mountains, New Hampshire. In: Van Baalen, M. (Ed.), Guidebook to Field Trips in Northern New Hampshire and Adjacent Regions of Maine and Vermont: New England Intercollegiate Geologic Conference, 88th Annual Meeting, pp. 203–225.
Thompson, W., Hildreth, C., Boisvert, R., Dorion, C., Fowler, B., 2002. Glacial geology and archaeology of the northern White Mountains, New Hampshire: Guidebook for the 65th annual reunion of the Northeastern Friends of the Pleistocene.
Williams, C., Menne, M., Vose, R., Easterling, D., 2007. United States Historical Climatology Network Available from: http://cdiac.ornl.gov/epubs/ndp/ushcn/newushcn.html.